Clim. Past Discuss., 7, 2445–2476, 2011
www.clim-past-discuss.net/7/2445/2011/
doi:10.5194/cpd-7-2445-2011
© Author(s) 2011. CC Attribution 3.0 License.

Climate of the Past Discussions

This discussion paper is/has been under review for the journal Climate of the Past (CP).
Please refer to the corresponding final paper in CP if available.

Climatically-controlled siliceous productivity in the eastern Gulf of Guinea during the last 40 000 yr

X. Crosta[1], O. E. Romero[2], O. Ther[1], and R. R. Schneider[3]

[1]EPOC, Environnements et Paléoenvironnements Océaniques et Continentaux, UMR5805, UMR-CNRS/INSU, Université Bordeaux 1, Talence Cedex, France
[2]Instituto Andaluz de Ciencias de la Tierra (CSIC-UGR), 18100, Armilla-Granada, Spain
[3]Marine Klimaforschung, Institut fuer Geowissenschaften, CAU Kiel, Germany

Received: 30 June 2011 – Accepted: 6 July 2011 – Published: 25 July 2011

Correspondence to: X. Crosta (x.crosta@epoc.u-bordeaux1.fr)

Published by Copernicus Publications on behalf of the European Geosciences Union.

Abstract

Opal content and diatom assemblages were analysed in core GeoB4905-4 to reconstruct siliceous productivity changes in the eastern Gulf of Guinea during the last 40 000 yr. Opal and total diatom accumulation rates presented low values over the considered period, except during the Last Glacial Maximum and between 12 000 calendar years (12 cal. ka BP) and 5.5 cal. ka BP, the so-called African Humid Period, when accumulation rates of brackish and freshwater diatoms to the core site were highest. Conversely, accumulation rates of windblown diatoms exhibited an opposite pattern with higher values before and after the African Humid Period and greatest values during Heinrich Events, the Younger Dryas and since 5.5 cal. ka BP.

Our results demonstrate that siliceous productivity in the eastern Gulf of Guinea was directly driven by the nutrient load from local rivers, which discharges were forced by precipitation over western Equatorial Africa. Precipitation in this region is controlled by the West African monsoon which is, in turn, dependent on the presence and intensity of the Atlantic Cold Tongue (ACT). The ACT was weakened and warmer, trade winds were less vigorous, could convection and precipitation were greater during the AHP though centennial-to-millennial timescale dry events were observed at ~10 cal. ka BP, ~8.5 cal. ka BP and ~6 cal. ka BP. Conversely, the ACT was more intense, trade winds were more vigorous and African climate was more arid during H1, the Younger Dryas and since 5.5 cal. ka BP. Our results therefore give indication on the ocean and atmosphere dynamics over the last 40 000 yr.

1 Introduction

A substantial part of the ocean's primary productivity is supported by diatoms (Tréguer et al., 1995). At the global ocean scale, diatom productivity primarily depends on the availability of dissolved silica (DSi) as diatoms need DSi to build their frustule. This explains why diatoms are dominant in coastal zones, the Southern Ocean and upwelling

CPD
7, 2445–2476, 2011

systems where high stocks of DSi exist. Dissolved silica stocks in coastal zones mainly result from sediment remobilisation and riverine input while DSi stocks in the Southern Ocean and upwelling systems are a consequence, at first order, of the marine silica cycle and global ocean circulation (Ragueneau et al., 2000). Conversely, diatoms are not competitive in oligotrophic tropical gyres where high sea-surface temperatures and low DSi stocks reduce silica uptake by diatoms (Hildebrand, 2000; Martin-Jézéquel et al., 2000).

Diatom production and burial in the Gulf of Guinea, defined as the part of the Atlantic Ocean northeast of a line running from Liberia to Gabon, are relatively low. Abundances hardly reach 1.10^7 diatoms per gram in surface sediments (Romero and Armand, 2010), which is 1–2 order of magnitude lower than diatom occurrences in the Southern Ocean (Crosta et al., 1997) and coastal upwellling systems (Romero et al., 2002; Abrantes et al., 2007). Diatom abundances in surface sediments of the Gulf of Guinea additionally demonstrate a westward decreasing gradient (Pokras and Molfino, 1986). Such distribution is related to low mean DSi concentrations in surface waters with values of ~2.5 µM in the western part of the Gulf of Guinea where DSi stocks originate from the nutrient-poor South Equatorial Counter Current (Peterson and Stramma, 1991) and ~8 µM in the eastern part of the Gulf of Guinea where rivers inject nutrient-rich freshwaters (Hugues et al., 2011). For comparison, mean DSi concentrations in surface waters of high latitudes of the Southern Ocean are ~60 µM (World Ocean Atlas, 2001). There is therefore a direct connection between DSi stocks and diatom production in surface waters and occurrence in sediments of the Gulf of Guinea and precipitation regimes over western Equatorial Africa.

Past changes in siliceous productivity were reconstructed on glacial-interglacial timescale in the east Equatorial Atlantic (Abrantes et al., 2003) and the Congo Fan from the southeast Atlantic (Uliana et al., 2002). In the east Equatorial Atlantic, variations in siliceous productivity and marine diatom assemblages were mainly related to the intensity of the equatorial upwelling. In addition, increased abundances of freshwater diatom *Aulacoseira* spp. and opal phytoliths further indicated enhanced aridity

CPD
7, 2445–2476, 2011

and transport intensity from central and East Africa to the marine realm during glacial times. In the southeast Atlantic off the Congo river, variations in siliceous productivity and marine diatom assemblages were related to the interplay of riverine discharges, controlled by changes in precipitation in western and central Equatorial Africa, and migrations of oceanic fronts, controlled by changes in wind regimes (Uliana et al., 2002; Marret et al., 2008).

Because of the absence of upwelling and proximity to the ITCZ, the eastern Gulf of Guinea may provide more straightforward information on climate changes in western Equatorial Africa than the eastern Equatorial Atlantic and the Congo Fan. Past changes in siliceous productivity has been there linked to local river discharges, forced by precipitation regime over western Equatorial Africa, though no real evidenced was provided (Weldeab et al., 2005, 2007b). Indeed, downcore records of diatom assemblages have never been produced for the eastern Gulf of Guinea. We here present diatom assemblages and opal content in core GeoB4905-4, located around 115 km to the southwest of the Sanaga River mouth, to assess (1) the dependency of diatom productivity to DSi delivered to the ocean by the local rivers and (2) climate changes, i.e. precipitation and wind regimes, during the last 40 000 yr at the centennial scale resolution.

2 Oceanographic and climatic settings

The sea-surface circulation in the eastern Equatorial Atlantic, driven by the atmospheric surface circulation, is governed by the South Equatorial Counter Current (SECC) that transports low nutrient saline waters towards the south (Peterson and Stramma, 1991). It is relayed by the Guinea Current (GC) that advects the low nutrient, saline waters into the Gulf of Guinea (Fig. 1). The GC is stronger during the boreal summer than the boreal winter. Surface waters exit to the south as the Angola Current (AC). Eventually, the AC transports southward a mix of warm, nutrient-poor surface waters and cool, upwelled waters from the Equatorial Under-Current (EUC) until the

CPD
7, 2445–2476, 2011

Angola-Benguela Front where it meets, at around 15° S, the northward surface drift from the Cape Basin.

The Niger and Sanaga rivers are the two main rivers flowing in the eastern Gulf of Guinea. They cover a catchment area of ~2 400 000 $km^3\,yr^{-1}$ and drive an annual riverine freshwater input of ~277 km^3 (Weldeab et al., 2007). More particularly, the drainage area of the Sanaga River is 133 000 km^2 and the mean annual discharge is 62 $km^3\,yr^{-1}$ (Kossoni et al., 2010). River discharges are minimal during the boreal winter-spring (February–April) and maximal during the boreal summer-autumn (July–November) with peak runoffs in September and October (Weldeab et al., 2007; Kossoni et al., 2010). Annual variations in the Sanaga discharge are determined by the yearly cycle of precipitations over Equatorial Africa, controlled by the West African monsoon (WAM). Atmospheric surface circulation in the Gulf of Guinea is dominated all year round by southwesterly trade winds (TW), which provide most of the moisture for the WAM (Lebel et al., 2009). The quantity of moisture available for the WAM is partly determined by the sea-surface temperature gradient between tropics and subtropics and, thus, the presence and extent of the Atlantic Cold Tongue (ACT) in the subtropical south Atlantic (Ruiz-Barradas et al., 2000). Warm sea-surface temperature anomalies in the Gulf of Guinea lead to greater evaporation and water vapour in the lower troposphere that, in turn, conducts to greater precipitation along the Guinean Coast. From a large-scale perspective, the WAM can be described in terms of the annual migration of the Inter-Tropical Convergence Zone (ITCZ). The ITCZ is located around 5–10° N and 15–20° N in western Equatorial Africa during the boreal winter and boreal summer, respectively, in response to the northward migration of the maximum of received solar radiation energy. Large precipitation over western Equatorial Africa, around 3000 mm yr^{-1} (Kossoni et al., 2010), support the presence of evergreen rainforest and savannah (Foley et al., 2003).

Dissolved silica in surface waters of the southwest Atlantic Ocean are around 2.5 µM (World Ocean Atlas, 2001) and, thus, bring very little nutrient to the eastern Gulf of Guinea. Dissolved silica concentrations in surface waters of the eastern Gulf of

CPD
7, 2445–2476, 2011

Guinea are slightly higher than in the open ocean with values of ~6–8 µM during the boreal summer (July–October) and ~2 µM during the boreal winter-spring (March–June) (Conkright et al., 2002). These variations appear related to the yearly cycle of discharge of local rivers that present mean concentrations of ~15 mg l^{-1} or ~230 µM (Boeglin et al., 2003; Hugues et al., 2011). High dissolved silica concentrations in African rivers are related to the prevalence of warm climate conditions that favour chemical weathering of crystalline rocks abundant on this continent (Dürr et al., 2011).

3 Material and methods

3.1 Stratigraphy

Gravity core GeoB4905-4 was retrieved during the Meteor cruise M41/1 in the eastern Gulf of Guinea (2°30′ N, 9°23.4′ E, 1328 m of water depth) around 115 km to the southwest of the Sanaga River mouth (Fig. 1). The age model of core GeoB4905-4 was based on fourteen ^{14}C-AMS datings of monospecific samples of the planktonic foraminifer *Globigerinoides rubber* pink and mixed planktonic foraminifers for the upper part of the core. Additional tuning points between the δ^{18}O *G. ruber* pink record and GISP2 δ^{18}O record allowed to extending the stratigraphy beyond the radiocarbon range. Radiocarbon ages were corrected for the mean marine reservoir age and calibrated to calendar ages using CALIB5 (Stuiver et al., 2005). The core covers the last 45.000 calendar years (cal. ka BP) in 1218 cm (Adegbie et al., 2003; Weldeab et al., 2005).

3.2 Diatom analysis

Diatom slides were prepared following the protocol outlined in Rathburn et al. (1997). Diatom identification was achieved on a Nikon 80i phase contrast microscope at a magnification of x1000. A minimum of 300 valves were identified, whenever possible,

CPD
7, 2445–2476, 2011

following the counting rules described in Crosta and Koç (2007). Several traverses across the coverslip were performed depending on valve adundances. Three cover slips per samples were examined. It was not possible to reach 300 diatom valves in samples between 12.5–13.3 cal. ka BP and 14.8–17.1 cal. ka BP.

Diatoms were identified to species or species group level, and the relative abundance of each species was determined as the fraction of the diatom species against total diatom abundance in the sample. Identification of marine diatoms was based on Sundström (1986), Moreno-Ruiz and Licea (1994), Moreno et al. (1996), Hasle and Syversten (1997), Romero et al. (1999), Rivera et al. (2006) and a suite of species-specific references. Identification of brackish and freshwater diatoms was based on Servant-Vildary (1981), Gasse (1986), Lange and Tiffany (2002), Sar et al. (2010) and a suite of species-specific references.

Diatom accumulation rates were calculated with the following equation

$$DAR = (Nv * WBD * SR)/2. \quad (1)$$

Where DAR are the diatom accumulation rates in millions cm^{-2} ka^{-1}, Nv are the number of diatom valves per gram of dry sediment, WBD is the wet bulk density in g cm^{-3} measured on board and SR are the sedimentation rates in cm ka^{-1}.

Diatom census counts were performed on the upper 932 cm of core GeoB4905-4 with a resolution of 4 cm from top to 372 cm and 8 cm from 372 cm to 932 cm, which provided a temporal resolution of 150–300 yr between 0.14–17 cal. ka BP and 200–400 yr between 17–31 cal. ka BP and ~500 between 31–40 cal. ka BP.

3.3 Ecological significance of diatoms

Around 80 diatom species or species groups were identified in core GeoB4905-4. To simplify this large dataset, species sharing similar ecology were lumped together. Previous investigations on diatom distribution in surface water and in surface sediments from low latitude environments have demonstrated that it was indeed possible to combine diatom species in several groups, based on habitats and nutrients and SST

CPD
7, 2445–2476, 2011

requirements. Identification of diatom groups in previous investigations were based on simple comparison of relative abundances or statistical approaches (Schuette and Schrader, 1981; Pokras et Molfino, 1986; Treppke et al., 1996; Schrader and Sorknes, 1997; Romero et Hebbeln, 2003; Jiang et al., 2004; Abrantes et al., 2007; Romero et al., 2009). We here built onto the publications cited above, summarized in Romero and Armand (2010), to identify three different marine water groups and one benthic/brackish water group. Additional diatom groups were identified according to diatom distribution in African rivers and lakes to account for freshwater diatoms and windblown diatoms (Servant-Vildary, 1978; Gasse, 1980a, b, 1986).

Tropical diatoms are thriving in warm, oligotrophic surface waters where siliceous productivity is low. This group is here dominated by large and highly silicified centric diatoms such as *Azpeitia* spp., *Planktonellia sol*, *Pseudosolenia calcaravis* and *Rhizosolenia* spp., *Thalassiosira* spp. with lesser occurrence of pennate diatoms such as *Nitzschia* spp. and *Thalassionema bacillare* (Table 1).

Meroplankton diatoms are living in nutrient-rich coastal marine environments but, generally, out of upwelling cells. This group tracks higher dissolved silica levels, higher siliceous productivity but low turbulence (no upwelling conditions). This group is here dominated by large and highly silicified centric diatoms such as *Actinocyclus* spp., *Actinoptychus* spp., *Coscinodiscus* spp., *Paralia sulcata* and the pennate species *Fragilariopsis doliolus* (Table 1). *Cyclotella* species, dominated here by *C. stylorum/litoralis* and *C. striata* occur both in coastal marine and coastal brackish environments (Lange and Syversten, 1989). The record of *Cyclotella* spp. in core GeoB4905-4 resembles to the record of meroplankton diatoms (Fig. 3), indicating that the two groups may share similar ecology in the study area. *Cyclotella* spp. were subsequently combined to the meroplankton group (Fig. 4).

Upwelling related diatoms are thriving in surface waters with high dissolved silica concentrations and/or high rate of nutrient replenishment to sustain blooming conditions. This group is here dominated by resting spores *Chaetoceros Hyalochaete* spp. (CRS) and *Thalassionema nitzschioides* var *nitzschioides* with accompanying

CPD
7, 2445–2476, 2011

occurrences of *Thalassionema nitzschioides* var *claviformis* (Table 1). It is possible that CRS are produced during the early upwelling phase after depletion of originally high nutrient levels while *Thalassionema nitzschioides* spp. occur later in the season when upwelling conditions are fading (Romero et al., 2002).

Diatoms of the benthic group are living attached to a substratum (rocks, sand, mud-flats, macrophytes, etc...) present in shallow, brackish waters of coastal zones and river mouths. This group is here dominated by pennate diatoms and, more particularly, by *Cocconeis* spp. (Table 1). This group tracks transport from the coast and/or river mouth to the core site (Pokras, 1991).

Freshwater diatoms are living in rivers beyond the marine influence. This group is here dominated by raphide pennate diatoms such as *Fragilaria* spp. and *Navicula* spp., which represent the benthic community of freshwater diatoms (Table 1). This group tracks river input to the eastern Gulf of Guinea and, ultimately, represents a record of the continental climate (Gasse et al., 1989; Romero and Hebbeln, 2003).

Windblown diatoms are limnobionthic diatoms that live in lakes from central and East Africa. This group is here dominated by centric diatoms, mainly *Aulacoseira* spp. with very low occurrences of *Stephanodiscus* spp. (Table 1). Lake diatoms can not be directly transported to the marine environment. *Aulacoseira* spp. are very abundant in emerged sediments of the dessicated paleolake Tchad and, thus, represents an indicator of wind deflation and transport intensity to the eastern Gulf of Guinea (Romero et al., 1999; Gasse, 2000).

3.4 Opal phytoliths analysis

Opal Phytoliths were fixed on permanent slides concomitantly to diatoms. Phytoliths were counted congruently to diatom census counts, and *n* specimens (0 minimum–13 maximum) were identified until diatom counts were completed. As such, the total number of phytoliths is dependent on the abundances of diatoms, as well as the abundances of opal phytoliths. Opal phytolith accumulation rates were calculated using the same formula than for diatoms.

CPD
7, 2445–2476, 2011

Taxonomic identification of opal phytoliths followed the nomenclature of Bukry (1980) and Bremond et al. (2008).

3.5 Ecological significance of phytoliths

Different shapes of opal phytoliths, formed inside the short cells of grass epidermis, prevail in different grass subfamilies. As such, phytoliths can be used to infer changes in vegetation cover. The Cross and Bilobate short cell types occur dominantly in the Panicoideae grass subfamily, the Saddle type mainly occur in the Chloridoieae grass subfamily, the Rondel and Trapezoiform polylobate types are mainly produced by the Pooideae grass subfamily (Bremond et al., 2008). The Cross, Bilobate and Saddle types are precipitated in C_4 grasses while Trapezoiform types are formed in C_3 grasses. In core GeoB4905-4, the opal phytolith assemblages are dominated by Cross and Bilobate types with minor occurrences of Saddle and Trapezoiform types.

Basically, opal phytoliths presence in marine sediments can be due to transport by rivers and winds. Phytoliths and freshwater diatoms in surface sediments in the Zaire fan region do not present the same distribution. Phytoliths accumulation rates are maximal 700 km offshore while freshwater diatom accumulation rates are maximal at the river mouth and decrease offshore (Jansen et al., 1989). This suggests a significant aeolian transport of opal phytoliths from the Namib desert to the ocean by southeast trade winds. Phytoliths were also found in aeolian dust collected at Mbour, Senegal (Skonieczny et al., accepted) along with *Aulacoseira* spp. and *Hantzschia amphioxys* and in sediment traps off western Africa (Romero et al., 1999). This information and the good agreement between the phytolith and the *Aulacoseira* gp records in core GeoB4905-4 (Fig. 3) argue for an aeolian origin of opal phytoliths in the eastern Gulf of Guinea.

CPD
7, 2445–2476, 2011

3.6 Biogenic opal analysis

Opal was determined with the sequential leaching technique developed by Müller and Schneider (1993). Reproducibility of the method is less than 2 %. Biogenic opal accumulation rates were calculated with the following equation

$$\text{OpalAR} = (\text{O} * \text{WBD} * \text{SR}). \quad (2)$$

Where Opal AR is the opal accumulation rate in $\text{g cm}^{-2}\,\text{ka}^{-1}$, O is the opal content of the sediment, WBD is the wet bulk density in g cm^{-3} measured on board and SR are the sedimentation rates in cm ka^{-1}.

4 Results

4.1 Biogenic opal

Biogenic opal accumulation rates varied between a minimum value of $\sim$0.2 $\text{g cm}^{-2}\,\text{ka}^{-1}$ at 15–16 cal. ka BP to a maximum value of 3.5 $\text{g cm}^{-2}\,\text{ka}^{-1}$ at 8–9 cal. ka BP (Fig. 3a, red line). Values were $\sim$1.5 $\text{g cm}^{-2}\,\text{ka}^{-1}$ during the period between 40 cal. ka BP and 22 cal. ka BP and $\sim$2 $\text{g cm}^{-2}\,\text{ka}^{-1}$ during the Last Glacial Maximum (LGM). Opal AR subsequently dropped to reach lowest values of $\sim$0.2 $\text{g cm}^{-2}\,\text{ka}^{-1}$ between 17 cal. ka BP and 15 cal. ka BP, when they started to increase again. The increasing pattern between 15 cal. ka BP and 8 cal. ka BP was interrupted by two lows centred at $\sim$13 cal. ka BP and $\sim$10 cal. ka BP. Opal AR subsequently decreased slightly between 8 cal. ka BP and 6 cal. ka BP, when they abruptly dropped to values of $\sim$0.8 $\text{g cm}^{-2}\,\text{ka}^{-1}$ that persisted during the last 5 cal. ka BP.

4.2 Diatom and phytolith accumulation rates

Total diatom accumulation rates (DAR) present the same pattern as opal AR during the last 40 cal. ka (Fig. 3a, black line). Values oscillated around 200×10^6 $\text{cm}^{-2}\,\text{ka}^{-1}$

CPD
7, 2445–2476, 2011

between 40 cal. ka BP and 22 cal. ka BP. Diatom AR increased to $\sim 500 \times 10^6$ cm^{-2} ka^{-1} during the LGM. Lowest diatom accumulation rates of $\sim 10 \times 10^6$ cm^{-2} ka^{-1} were observed during the 17–15 cal. ka BP period. Diatom AR increased again at 15 cal. ka BP to reach a maximum of $\sim 850 \times 10^6$ cm^{-2} ka^{-1} centred at 7.5 cal. ka BP. High DAR values were recorded until 5.7 cal. ka BP when they abruptly dropped to reach low values of $\sim 150 \times 10^6$ cm^{-2} ka^{-1} that persisted during the last 5 cal. ka. Millennial-scale events of low occurrences centred at 13 cal. ka BP, 10 cal. ka BP, 8.5 cal. ka BP and 6 cal. ka BP interrupted the period of highest DAR.

Tropical diatoms presented very low AR between 40 cal. ka BP and 12.5 cal. ka BP, although a small increase occurred during the earliest phase of the LGM (Fig. 3b). Tropical diatom AR presented values above $\sim 100 \times 10^6$ cm^{-2} ka^{-1} between 12.5 cal. ka BP and ~5 cal. ka BP. Highest DAR around 350×10^6 cm^{-2} ka^{-1} were recorded at ~7.5 cal ka NP. Centennial-scale events of low occurrences centred at ~10 cal. ka BP, ~8.5 cal. ka BP and ~6 cal. ka BP interrupted the period of high accumulation rates of tropical diatoms. Very low AR values were again recorded since ~5 cal. ka BP.

Accumulation rates of meroplanktonic diatoms (Fig. 3c, black line), *Cyclotella* spp. (Fig. 3c, grey line) and upwelling-related diatoms (Fig. 3d) present a similar pattern during the last 40 cal. ka BP than observed for total DAR (Fig. 3a, black line). Centennial-scale events of low AR centred at ~20 cal. ka BP, ~13 cal. ka BP, ~10 cal. ka BP, ~8.5 cal. ka BP and ~6 cal. ka BP are similarly apparent. Accumulation rates of meroplanktonic diatoms, *Cyclotella* spp. and upwelling-related diatoms presented variability of higher amplitude during the 40–18 cal. ka BP period than observed for total DAR and tropical diatom AR.

Accumulation rates of freshwater (Fig. 3e, black line) and benthic (Fig. 3e, grey line) diatoms co-vary during the last 40 cal. ka BP. They present low values until the LGM when they abruptly increased. A short-lived drop in freshwater and benthic AR occurred at ~20 cal. ka BP. Accumulation rate values were low again between 18 cal. ka BP and 15 cal. ka BP when they started to increase to reach maximum values at ~7.5 cal. ka BP. Centennial-scale events of low occurrences centred at ~13 cal. ka

CPD
7, 2445–2476, 2011

BP, ~10 cal. ka BP, ~8.5 cal. ka BP and ~6 cal. ka BP interrupted the period of highest freshwater and benthic diatom AR.

Accumulation rates of windblown diatoms (Fig. 3f, black line) and opal phytoliths (Fig. 3f, grey line) present a similar evolution between 40 cal. ka BP and 4 cal. ka BP. Low AR values were generally observed throughout this period except during Heinrich Events (HE), a short-lived event centred at ~20 cal. ka BP and the Younger Dryas (YD). Low values were also observed during the 13–5 cal. ka BP period when highest DAR and opal AR were recorded. After 5 cal. ka BP, AR of windblown diatoms and phytoliths differ, with high occurrences of windblown diatoms and continuously low occurrences of opal phytoliths.

4.3 Diatom relative abundances

The relative contribution of each group to total diatom assemblages is depicted in Fig. 4. During the 40–35 cal. ka BP period, tropical diatoms, meroplanktonic diatoms and upwelling diatoms amounted for ~95 % of the diatom assemblages, while freshwater and benthic diatoms accounted for ~5 %. Windblown diatoms were absent except for a short-lived occurrence at ~36 cal. ka BP. After 35 cal. ka BP, the contribution of tropical diatoms decreased slightly, the contribution of meroplanktonic diatoms decreased sharply (mainly because of less abundant *Cyclotella litoralis/stylorum*), while the contribution of upwelling-related diatoms increased. Freshwater and benthic diatoms were still present at low percentages while windblown diatoms occurred episodically at percentages below 2 %. An increase in both tropical and meroplanktonic diatoms was recorded between 22 cal. ka BP and 17.5 cal. ka BP at the expense of upwelling-related diatoms. A very abrupt and pronounced decrease in marine diatoms occurred subsequently between 17.5 cal. ka BP and 15 cal. ka BP. During this period marine diatoms, produced locally, accounted for less than 50 % of the assemblage. The other fraction of the diatom assemblage was mainly represented by windblown diatoms with accompanying freshwater and benthic diatoms. However, the contribution of freshwater/benthic diatoms and windblown diatoms were out-of-phase during this

CPD
7, 2445–2476, 2011

event as identified in the AR records (Fig. 3e and f). It is worth noting that less than 50 diatom valves per sample could be counted during this period. A second similar event, though much less pronounced, was observed between 12.5 cal. ka BP and 13.5 cal. ka BP. Here again, highest contribution of freshwater and benthic diatoms occurred just before and immediately after the peak abundance of windblown diatoms. Around 50–80 diatom valves per sample could be counted during this period.

Between 12.5 cal. ka BP and 5 cal. ka BP, the period of highest accumulation rates in core GeoB4905-4, tropical diatoms increased to account for ~40 % of the diatom assemblages. Meroplanktonic diatoms accounted for ~10–15 % while upwelling-related diatoms decreased to ~30 % of the diatom assemblage. Freshwater and benthic diatoms concomitantly represented ~5–10 % of the assemblages while windblown diatoms were totally absent. After ~5 cal. ka BP, both tropical and meroplanktonic diatom abundances dropped while abundances of upwelling-related diatoms increased to ~45 % of the assemblages. Freshwater and benthic diatoms almost disappeared while windblown diatoms congruently increased to ~3 % of the diatom assemblages.

5 Discussion

5.1 Diatom productivity during the last 40 cal. ka BP

The low range of sedimentation rates and sediment density values in core GeoB4905-4 (Fig. 2) indicates that variations in biogenic opal and diatom AR reflect changes in siliceous productivity. DAR and opal AR records demonstrated relatively low siliceous productivity during the 40–22 cal. ka BP period, higher productivity during the LGM, extremely low productivity during the 19–15 cal. ka BP period, high productivity during the 15–5.5 cal. ka BP and, eventually, low productivity since 5.5 cal. ka BP (Fig. 5a). Siliceous productivity was highest during the 13–5.5 cal. ka BP period, i.e. during the African Humid Period (AHP) (deMenocal et al., 2000). Variations in siliceous productivity over the last 40 cal. ka were congruent to changes in accumulation rates of

CPD
7, 2445–2476, 2011

freshwater (Fig. 3e, black line) and benthic (Fig. 3e, grey line) diatoms. The positive relationship between opal AR and freshwater diatom AR, and the fact that highest DAR and opal AR occurred during the AHP, suggests that diatom productivity in the eastern Gulf of Guinea is supported by DSi input from local river discharges rather than DSi transported by the GC and EUC. Siliceous productivity was therefore indirectly controlled by precipitation variations over western Equatorial Africa. Short lived drops in siliceous productivity, superimposed to the long trend, occurred at ~20 cal. ka BP during the LGM, ~16 cal. ka BP during H1, ~13 cal. ka BP during the YD, ~10 cal. ka BP, ~8.5 cal. ka BP and ~6 cal. ka BP. These drops probably represented less DSi availability and, thus, more arid conditions over western Equatorial Africa.

Greater availability of DSi particularly favoured sub-tropical diatoms that increased by 10 % and 20 % during the LGM and AHP, respectively, compared to their relative contribution during MIS 3 (Fig. 4). Conversely, relative abundances of upwelling-related diatoms decreased during the LGM and AHP. Upwelling-related diatoms are fast blooming diatoms (Hargraves, 1972) thriving in coastal, nutrient-rich and relatively cold environments due to the resurgence of intermediate-to-deep waters (Romero and Armand, 2010). Tropical diatoms are conversely slow-developing, large and heavily silicified diatoms thriving in warm surface waters (Romero et al., 1999) in comparison to upwelling-related diatoms. Today, the decreasing gradient in diatom abundances towards the western Gulf of Guinea may indicate that upwelling-related diatoms outcompete sub-tropical diatoms and uptake most of the DSi injected by rivers in the eastern Gulf of Guinea, thus preventing development of sub-tropical diatoms. Warmer SST during the early Holocene may have been less favourable to upwelling-related diatoms while more favourable to tropical diatoms that could extend their distribution and could make use of the higher DSi stocks.

After the termination of the AHP at 5.5 cal. ka BP, drier, windier and cooler conditions may have induced upwelling-like conditions in the eastern Gulf of Guinea but less nutrient input by local rivers, which was unfavourable to sub-tropical diatoms. As a result, relative abundances of upwelling-related diatoms increased while relative abundances

CPD
7, 2445–2476, 2011

of sub-tropical diatoms decreased. Diatom AR and assemblages did not show drastic changes since 5.5 cal. ka BP, though a more detailed investigation of the last centuries would be necessary to document how the recent warming of the ACT and greater precipitation over the coast of the Gulf of Guinea have impacted diatom communities.

5.2 Precipitation changes in western Equatorial Africa during the last 40 cal. ka BP

The diatom records in core GeoB4905-4 (Fig. 3) demonstrate highest precipitation over western Equatorial Africa during the LGM and the AHP, and lowest precipitation during HEs and the YD. Short-lived dry spells occurred at ~20 cal. ka BP, ~10 cal. ka BP, ~8.5 cal. ka BP and ~6 cal. ka BP., thus interrupting the LGM and the AHP. Lowest precipitation was estimated during the HEs and the YD.

Our results are supported by marine records from the Equatorial Atlantic and continental records from Equatorial Africa. Record of sea-surface salinities (Weldeab et al., 2005) in core GeoB4905-4 demonstrated high salinities during the 22–15 cal. ka BP and 5.5–0 cal. ka BP periods while low salinities were encountered during the 15–5.5 cal. ka BP (Fig. 5c). Highest salinities were observed during H1 and the YD, while lowest salinities were recorded during 12–7 cal. ka BP period.

Records of fluvial delivery (Weijers et al., 2009) and continental rainfall (Schefuss et al., 2005; Marret et al., 2008) in cores located at the mouth of the Congo River (Fig. 1), provided additional insight on regional freshwater discharges to the eastern Gulf of Guinea. All together these marine records argued for higher precipitation and river discharges during the AHP and lower precipitation and discharges before and after the AHP (Fig. 5). Over the last 40 000 yr, lowest precipitation and river discharges occurred during H1 and the YD.

A phase lag is present between records from core GeoB4905-4 and records from cores located at the mouth of the Congo River. Disregarding dating uncertainties, this phase lag may indicate that past precipitation dynamics over the basins drained by the

CPD
7, 2445–2476, 2011

Sanaga and Congo rivers were slightly different or that the impact of river discharges onto the marine environment was different. First, the Congo drainage basin is influenced by both the WAM and the East African Monsoon (Gasse, 2000; Tierney et al., 2011) while the Sanaga drainage basin is essentially influenced by the WAM. Second, southeastern trade winds promote a seasonal upwelling off the Congo River that does not occur in the eastern Gulf of Guinea (Uliana et al., 2002; Marret et al., 2008). Enhanced upwelling during times of stronger trade winds generally intensified marine paleoproductivity in the Congo fan area during cold stages, but strongest river discharges also yield to upwelling of nutrient rich sub-surface waters during warm stages (Kim et al., 2010).

African lake level fluctuations give further indication on Equatorial Africa climate variability. Lake Abhé (Fig. 5g, black curve) in eastern Equatorial Africa evidenced high precipitation during the Marine Isotope Stage 3 (MIS 3) and the earliest phase of the LGM, and reduced precipitation during HEs and at ~20 cal ka. BP. Lake Abhé subsequently dried out until ~15 cal. ka BP (Gasse et al., 1989; Talbot and Livingston, 1989), thus demonstrating a drastic reduction in precipitation during this period in agreement with diatom records in core GeoB4905-4. Lake Abhé and lake Bar-El-Ghazal (Fig. 5g, red curve) in central Equatorial Africa had highest lake levels during the 11.5–5 cal. ka BP period, in good agreement with records of freshwater and benthic diatoms in core GeoB4905-4. Two prominent dessication events occurred at ~8.5 cal. ka BP and 6.5 cal. ka BP (Fig. 5g, black curve) in phase with the dry spells interrupting the AHP as evidenced by the diatom records. Lake levels sharply dropped at 5 ka BP. These results suggest that the precipitation changes inferred from the diatom records in core GeoB4905-4 affected the whole Equatorial Africa as part as large scale climate changes.

CPD
7, 2445–2476, 2011

5.3 Forcing of precipitation changes in Equatorial Africa during the last 40 cal. ka BP

Precipitation over western Equatorial Africa is controlled by the WAM. The quantity of moisture available for the WAM is partly determined by the sea-surface temperature gradient between tropics and subtropics and, thus, the presence and extent of the Atlantic Cold Tongue (ACT) in the subtropical south Atlantic (Thorncrof et al., 2011). Warm sea-surface temperature anomalies in the Gulf of Guinea lead to greater evaporation and water vapour in the lower troposphere that, in turn, conducts to greater precipitations along the Guinean Coast (Lebel et al., 2009). Historical observations of meteorological measurements along ships lanes in the Equatorial Atlantic have shown that the ACT weakened and warmed by 1.5 °C over the last sixty years (Tokinaga et al., 2011). This SST warming reduced southwesterly trade winds intensity and enhanced marine cloud cover over Equatorial Atlantic and land precipitation over western Equatorial Africa during the boreal summer season.

Based on the modern observations depicted above, we expect a causal relationship between SST in the eastern Equatorial Atlantic and precipitation regimes in western Equatorial Africa during the last 40 cal. ka BP (Fig. 5). We also expect a positive correlation between the SST record in core GeoB4905-4 (Weldeab et al., 2007) and our records of freshwater and benthic diatom accumulation rates, and a negative correlation between the SST record and the records of windblown microfossils (Fig. 3).

The SST record in core GeoB4905-4 showed strong variability during the LGM with a pronounced cooling event at ∼20 ka BP interrupting warmer periods. Freshwater and benthic DAR during the LGM "warm" periods were relatively high and dropped abruptly during the cooling event (Fig. 3f). Conversely, accumulation rates of windblown microfossils were very low during the LGM "warm" periods and increased drastically during the LGM cool event. Similarly, H1 and the YD were periods of cool surface water temperatures interrupting the deglaciation warming in the eastern Gulf of Guinea. Our diatom records argued for congruent arid conditions. Highest SST in the eastern Gulf

CPD
7, 2445–2476, 2011

of Guinea were recorded during the 12–5.5 ka BP period when greatest freshwater and benthic DAR rates were observed while windblown diatoms and opal phytoliths were almost absent. During the Holocene, millennial-scale events of warmer (colder) surface waters in the Gulf of Guinea were congruent with greater (lower) freshwater DAR. Lower SST since 5 cal. ka BP were in phase with lower freshwater DAR and greater windblown material AR.

The SST record in core GeoB4905-4 therefore suggests that the ACT was reduced during the AHP in terms of intensity and extent with temperature ~2 °C above the pre-industrial mean. Weakened and warmer ACT yielded to less vigorous southwesterly trade winds, greater cloud convection and greater precipitation in western Equatorial Africa at the origin of greater nutrient-rich freshwater input to the eastern Gulf of Guinea. Variations in the ACT intensity and extent may have interplayed with the tropical-subtropical SST gradient in the South Atlantic Ocean (Scheffus et al., 2005) and the land-sea thermal gradient (Weijers et al., 2003) that were suggested to exert a strong control on precipitation changes over central Africa.

6 Conclusions

Analyses of biogenic opal and diatom assemblages in core GeoB4905-4, located 115 km southwest of the mouth of the Sanaga River, demonstrate that siliceous productivity changes in the eastern Gulf of Guinea during the last 40 cal. ka BP was controlled by the dissolved silica delivered by local rivers to the ocean. Siliceous productivity was therefore indirectly controlled by precipitation variations over western Equatorial Africa. Precipitation was more intense during the African Humid Period (15–5 cal. ka BP) though centennial-to-millennial timescale dry events were observed at ~13 cal. ka BP, ~10 cal. ka BP, ~8.5 cal. ka BP and ~6 cal. ka BP. The Last Glacial Maximum (LGM) was also relatively wet in western Equatorial Africa, though it was interrupted by a 1500 yr dry event centred at ~20 cal. ka BP. Especially dry conditions occurred during H1, the Younger YD and since 5.5 cal. ka BP as evidenced by the presence

CPD
7, 2445–2476, 2011

of windblown diatoms and phytolithes in the core during these intervals. Precipitation changes were linked to variations in the west African monsoon regime, partly forced by variations in intensity and extent of the Atlantic cold Tongue. Diatoms did not record important changes in precipitation during 40 cal. ka BP and the LGM, indicating more stable, relatively arid conditions during this period.

Warmer sea-surface temperatures and greater discharge of dissolved silica during the early Holocene promoted the development of tropical oceanic diatoms at the expense of coastal, upwelling-related diatoms. Tropical diatoms are large and highly silicified, and their export to the sediment resulted in the high opal accumulation during the early Holocene.

Acknowledgements. We thank Bruno Malaizé for constructive discussions and Fabienne Marret for data. We also thank x reviewers for helpful comments that improved the manuscript. CX was funded by Financial support for this study was provided by CNRS (Centre national de la Recherche Scientifique), while OE and RS were funded by DFG (Deutsche Forschungsgemeinschaft). This is an EPOC contribution N° x.

The publication of this article is financed by CNRS-INSU.

References

Abrantes, F.: A 340,000 year continental record from tropical Africa – News from opal phytoliths from the equatorial Atlantic, Earth Planet. Sci. Lett., 209, 165–179, 2003.

Abrantes, F., Lopes, C., Mix, A., and Pisias, N.: Diatoms in southeast Pacific surface sediments reflect environmental properties, Quat. Sci. Rev., 26, 155–169, 2007.

CPD
7, 2445–2476, 2011

Adegbie, A. T., Schneider, R. R., Röhl, U., and Wefer, G.: Glacial millennial-scale fluctuations in central African precipitation recorded in terrigenous sediment supply and freshwater signals offshore Cameroon, Palaeogeogr., Palaeoclimatol., 197, 323–333, 2003.

Boeglin, J. L., Ndam, J. R., and Braun, J. J.: Composition of the different reservoir waters in a tropical humid area: Example of the Nsimi catchment (Southern Cameroon), J. Afr. Earth Sci., 37, 103–110, 2003.

Bremond, L., Alexandre, A., Wooller, M.J., Hély, C., Williamson, D., Schäfer, P.A., Majule, A., and Guiot, J.: Phytolith indices as proxies of grass subfamilies on East African tropical mountains, Global Planet. Change, 61, 209–224, 2008.

Bukry, D.: Opal phytoliths from the tropical eastern Pacific Ocean, Deep Sea Drilling Project Leg 54, in: Initial Reports of the Deep Sea Drilling Project., edited by: Rosendahl, B. R. and Hekinian, R. , US Govt. Printing Office, Washington, D. C, 575–590, 1980.

Crosta, X. and Koç, N.: Diatoms: From micropaleontology to isotope geochemistry, in Hilaire-Marcel, C, and de Vernal, A. (Eds.), Proxies in Late Cenozoic Paleoceanography, Elsevier, Amsterdam, The Netherlands, 327–369, 2007.

Crosta, X., Pichon, J. J., and Labracherie, M.: Distribution of Chaetoceros resting spores in modern peri-Antarctic sediments, Mar. Micropaleontol., 29, 238–299, 1997.

deMenocal, P., Ortiz, J., Guilderson, T., and Sarnthein, M.: Coherent high- and low-latitude climate variability during the Holocene warm period, Science, 288, 2198–2202, 2000.

Dürr, H. H., Meybeck, M., Hartmann, J., Laruelle, G. G., and Roubeix, V.: Global spatial distribution of natural riverine silica inputs to the coastal zone, Biogeosciences, 8, 597–620, doi:10.5194/bg-8-597-2011, 2011.

Foley, J. A., Coe, M. T., Scheffer, M., and Wang, G.: Regime shifts in the Sahara and Sahel: Interactions between ecological and climatic systems in Northern Africa, Ecosystems, 6, 524–539, 2003.

Gasse, F. : Les diatomées lacustres plio-pléistocène du Gadeb (Ethipie). Systématique, paléoécologie, biostratigraphie, Revue d'Algologie, Mémoire Hors-Série, 3, pp. 249, 262 pls, 1980a.

Gasse, F.: East African diatoms: Taxonomy, ecological distribution. J. Cramer, Berlin, Germany, pp. 201, 44 pls., 1980b.

Gasse, F.: Hydrological changes in the African tropics since the Last Glacial Maximum, Quat. Sci. Rev., 19, 189–211, 2000.

Gasse, F., Stabell, B., Fourtanier, E., and van Iperen, Y.: Freshwater diatom influx in intertrop-

CPD
7, 2445–2476, 2011

ical Atlantic: Relationhsips with continental records from Africa, Quaternary Res., 32, 229–243, 1989.
Hargraves, P. E.: Studies on marine plankton diatoms. I. Chaetoceros diadema (Ehr.) Gran: life ecycle, structural morphology, and regional distribution, Phycologia, 11(3-4), 205-215, 1972.
Hasle, G. R. and Syversten, E. E.: Marine diatoms, in Tomas, C.R. (Eds.), Identifying Marine Diatoms and Dinoflagellates, Academic Press, San Diego, USA, 5–385, 1997.
Hildebrand, M.: Silicic acid transport and its contron during cell wall silicification in diatoms, in: Biomineralization – From biology to biotechnology and medical applications, edited by: Baüerlein, E., Wiley-VCH, Weinheim, Germany, 170–188, 2000.
Hugues, H. J., Sondag, F., Cocquyt, C., Laraque, A., Pandi, A., André, L., and Cardinal, D.: Effect of seasonal biogenic silica variations on dissolved silicon fluxes and isotopic signatures in the Congo River, Limnol. Oceanogr., 556(2), 551–561, 2011.
Jansen, J. H. F., Alderliesten, C., Houston, C. M., Dejong, A. F. M., Vanderborg, K., and van Iperen, J. M.: Aridity in equatorial Africa during the last 225,000 years – A record of opal phytoliths/fresh-water diatoms from the Zaire (Congo) deep-sea fan (Northeast Angola Basin), Radiocarbon, 31, 557–596, 1989.
Jiang, H., Zheng, Y., Ran, L., and Seidenkrantz, M. S.: Diatoms from the surface sediments of the South China sea and their relationships to modern hydrography, Mar. Micropaleontol., 53, 279–292, 2004.
Kim, S. Y., Scourse, J., Marret, F., and Lim, D. I.: A 26,000-year integrated record of marine and terrestrial environmental change off Gabon, west equatorial Africa, Palaeogeogr. Palaeoclimatol., 297(2), 428–438, 2010.
Kossoni, A. and Giresse, P.: Interaction of Holocene infilling processes between a tropical shallow lake system (Lake Ossa) and a nearby river system (Sanaga River) (South Cameroon), J. Afri. Earth Sci., 56, 1–14, 2010.
Lange, C. B. and Syversten, E. E.: *Cyclotella litoralis* sp. nov. (Bacillariophyceae), and its relationships to *C. striata* and *C. stylorum*, Nova Hedwigia, 48(3–4), 341–356, 1989.
Lange, C. B. and Tiffany, M. A.: The diatom flora of the Salton Sea, California, Hydrobiologia, 473, 179–201, 2002.
Lebel, T. and Ali, A.: Recent trends in the Central and Western Sahel rainfall regime (1990–2007), J. Hydrol., 375, 52–64, 2009.
Marret, F., Scourse, J., Kennedy, H., Ufkes, E., and Jansen, J. H. F.: Marine production in the Congo-influenced SE Atlantic over the past 30,000 years: A novel dinoflagellate-cyst based

CPD
7, 2445–2476, 2011

transfer function approach, Mar. Micropaleontol., 68, 198–222, 2008.
Martin-Jézéquel, V., Hildebrand, M., and Brzezinski, M. A.: Silicon metabolism in diatoms: Implications for growth, J. Phycol., 36, 821–840, 2000.
Moreno, J. L., Licea, S., and Santoyo, H.: Diatomeas del Golfo de California, Universidad Autonoma de Baja california Sur, Mexico, Mexico, pp. 203, 34 pls., 1996.
Moreno-Ruiz, J. L. and Licea, S.: Observations on the valve morphology of *Thalassionema nitzschoides* (Grunow) Hustedt, in: Proceedings of the 13th Symposium on Living and Fossil Diatoms, edited by: Marino, D. and Montresov, M., Biopress Limited Publisher, Bristol, Maretea, Italy, 1–7 September, 1994, 393–413, 1994.
Müller, P. J. and Schneider, R.: An automated leaching method for the determination of opal in sediments and particulate matter, Deep Sea Res. I, 40(3), 425–444, 1993.
Peterson, R. G. and Stramma, L.: Upper-level circulation in the South Atlantic Ocean, Progr. Oceanogr., 26(1), 1–73, 1991.
Pokras, E. M.: A displaced diatom (*Delphineis karstenii*) in pelagic sediments of the southeast Atlantic, Mar. Micropaleontol., 17, 311–317, 1991.
Pokras, E. M. and Molfino, B.: Oceanographic control of diatom abundances and species distribution in surface sediment of the Tropical and Southeast Atlantic, Mar. Micropaleontol., 10, 165–188, 1986.
Ragueneau, O., Tréguer, P., Leynaert, A., Anderson, R. F., Brzezinski, M. A., DeMaster, D. J., Dugdale, R. C., Dymont, J., Fischer, G., François, R., Heinze, C., Maier-Riemer, E., Martin-Jézéquel, V., Nelson, D. M., and Quéguiner, B.: A review of the Si cycle in the modern ocean: Recent progress and missing gaps in the application of biogenic opal as a paleoproductivity proxy, Global Planet. Change, 26, 317–365, 2000.
Rathburn, A. E. and Deckker, P. D.: Magnesium and strontium compositions of recent benthic foraminifera from the Coral Sea, Australia and Prydz Bay, Antarctica, Mar. Micropaleontol., 32, 231–248, 1997.
Rivera, P., Cruces, F., and Avaria, S.: *Thalassionema bacillare* (Heiden) Kolbe (Thalassionemataceae, Bacillariophyceae): Una especia ahora casi desconocida para las aguas chilenas pero comun en el fitoplancton costero de la zona norte, Ciencias y Tecnologias Marinas, 29(1), 59–70, 2006.
Romero, O. E. and Armand L. K.: Marine diatoms as indicators of modern changes in oceanographic conditions, in: The diatoms: Applications for the Environmental an d Earth Sciences, edited by: Smol, J. P. and Stoermer, E. F., Second Edition, 373–400, 2010.

CPD
7, 2445–2476, 2011

Romero, O. E. and Hebbeln, D.: Biogenic silica and diatom thanatocoenosis in surface sediments below the Peru-Chile Current: Controlling mechanisms and relationship with productivity of surface waters, Mar. Micropaleontol., 48, 71–90, 2003.

Romero, O. E., Boeckel, B., Donner, B., Lavik, G., Fischer, G., and Wefer, G.: Seasonal productivity dynamics in the pelagic central Benguela system inferred from the flux of carbonate and silicate organisms, J. Mar. Syst., 37, 259–278, 2002.

Romero, O. E., Rixen, T., and Herunadi, B.: Effects of hydrographic and climatic forcing on diatom production and export in the tropical southeastern Indian ocean, Mar. Ecol.-Progr. Ser., 384, 69–82, 2009.

Romero, O. E., Lange, C. B., Fisher, G., Treppke, U. F., and Wefer, G.: Variability in export production documented by downward fluxes and species composition of marine planktic diatoms: Observations from the Tropical and Equatorial Atlantic, in: Use of Proxies in Paleoceanography: Examples from the South Atlantic, edited by: Fisher, G. and Wefer, G., Springer-Verlag, Berlin Heidelberg, Germany, 365–392, 1999.

Ruiz-Barradas, A., Carton, J. A., and Nigam, S.: Structure of interannual-to-decadal climate variability in the tropical Atlantic sector, J. Climate, 13, 3285–3297, 2000.

Sar, E. A., Sunesen, I., and Lavigne, A. S.: *Cymatotheca*, *Trybliоptychus*, *Skeletonema* and *Cyclotella* (Thalassiosirales) from Argentinian coastal waters. Description of *Cyclotella cubiculata* sp. nov., Vie et Milieu, 60(2), 135–156, 2010.

Schefuss, E., Schouten, S., and Schneider, R.: Climatic controls on central African hydrology during the past 20.000 years, Nature, 437, 1033–1006, 2005.

Schrader, H. and Sorknes, R.: Peruvian coastal upwelling: Late Quaternary productivity changes revealed by diatoms, Mar. Geol., 97, 233–249, 1991.

Schuette, G. and Schrader, H.: Diatom taphocoenoses in the coastal upwelling area off south west Africa, Mar. Micropaleontol., 6, 131–155, 1981.

Servant-Vildary, S. : Etudes des diatomées et paléolimnologie du bassin tchadien au Cénozoique Supérieur, Travaux et Documents de l'ORSTOM, 84 (2 vol.), pp. 345, 1978.

Skonieczny, C., Bory, A., Bout-Roumazeilles, V., Abouchami, W., Galer, S. J. G., Crosta, X., Stuut, J. B., Meyer, I., Chiapello, I., Podvin, T., Chatenet, B., Diallo, A., and Ndiaye, T. : Mineral dust deposition multi-proxy characterization during a major Saharan spring outbreak, J. Geophys. Res., accepted, 2011.

Stuiver, M., Reimer, P. J., and Reimer, R. W.: CALIB 5.0 [WWW program and documentation], 2005.

CPD
7, 2445–2476, 2011

Sundström, B. G.: The marine diatom genus *Rhizosolenia*. A new approach to the taxonomy, Ph.D. Thesis, University of Lund, Sweden, pp. 116, 39 pls., 1986.
Talbot, M. R. and Livingstone, D. A.: Hydrogen index and carbon isotopes of lacustrine organic matter as lake-level indicators, Palaeogeogr., Palaeoclimatol., 80, 283–300, 1989.
Thorncroft, C. D., Nguyen, H., Zhang, C., and Peyrillé, P.: Annual cycle of the West African monsoon: Regional circulations and associated water vapour transport, Q. J. Roy. Meteorol. Soc., 137 (Part A.), 129–147, 2011.
Tierney, J. E., Russell, J. M., Sinninghe Damsté, J. S., Huang, Y., and Verschuren, D.: Late Quaternary behavior of the East African monsoon and the importance of the Congo Air Boundary, Quat. Sci. Revi., 30, 798–807, 2011.
Tokinaga, H. and Xie, S. P.: Weakening of the equatorial Atlantic cold tongue over the past six decades, Nat. Geosci., 4, 222–226, 2011.
Tréguer, P., Nelson, D. M., van Bennekom, A. J., DeMaster, D. J., Leynaert, A., and Quéguiner, B.: The silica balance in the world ocean, Science, 268, 375–379, 1995.
Treppke, U. F., Lange, C. B., and Wefer, G.: Vertical fluxes of diatoms and silicoflagellates in the eastern equatorial Atlantic, and their contribution to the sedimentary record, Mar. Micropaleontol., 28, 73–96, 1996.
Uliana, E., Lange, C. B., and Wefer, G.: Evidence for Congo River freshwater load in Late Quaternary sediments of ODP Site 1077 (5° S, 10° E), Palaeogeogr., Palaeoclimatol., 187, 137–150, 2002.
Weijers, J. W. H., Schefuss, E., Schouten, S., and Sinninghe Damsté, J. S.: Coupled thermal and hydrological evolution of the tropical Africa over the last deglaciation, Science, 315, 1701–1704, 2003.
Weijers, J. W. H., Schouten, S., Schefuss, E., Schneider, R. R., and Sinninghe Damsté, J. S.: Disentangling marine, soil and plant organic carbon contributions to continental margin sediments: A multi-proxy approach in a 20,000 year sediment record from the Congo deep-sea fan, Geochim. Cosmochim. Ac., 73, 119–132, 2009.
Weldeab, S., Schneider, R. R., Kölling, M., and Wefer, G.: Holocene African droughts relate to eastern equatorial Atlantic cooling, Geology, 33(12), 981–984, 2005.
Weldeab, S., Schneider, R. R., and Müller, P.: Comparison of Mg/Ca- and alkenone-based sea surface temperatures estimates in the fresh water-influenced Gulf of Guinea, eastern equatorial Atlantic, Geochem. Geophys. Geosy., 8(5), Q05P22, doi:10.1029/2006GC001360, 2007a.

CPD
7, 2445–2476, 2011

Weldeab, S., Lea, D. W., Schneider, R. R., and Andersen, N.: Centennial scale climate instabilities in a wet early Holocene West African monsoon, Geophys. Res. Lett., 34, L24702, doi:10.1029/2007GL031898, 2007b.

World Ocean Atlas 2001: Objective Analyses, Data Statistics, and Figures, CD-ROM documentation, US Dept. of Comm., Washington, D. C, 2001.

CPD

7, 2445–2476, 2011

Table 1. List of diatom species or species groups included in the different groups. Diatom group identification and diatom species assignment are detailed in the text.

Tropical diatoms	Meroplankton diatoms	Upwelling diatoms	Benthic/brackish diatoms	Freshwater diatoms	Windblown diatoms
Alveus marinus	*Actinocyclus* spp.	*Chaetoceros Hyalochaete* resting spores	*Achnantes* spp.	*Fallacia pygmaea*	*Aulacoseira granulata*
Azpeitia africana	*Actinocyclus curvatulus*		*Amphora* spp.	*Fragilaria construens*	*Aulacoseira gotzeana*
Azpeitia nodulifera	*Actinocyclus octonarius*	*Thalassionema nizschioides* var *capitula*	*Catenula* spp.	*Fragilaria parasitica*	*Stephanodiscus* spp.
Azpeitia tabularis	*Actinoptychus* spp.		*Cocconeis* spp.	*Fragilaria pinnata*	
Bacteriastrum spp.	*Actinoptychus senarius*	*Thalassionema nizschioides* var *claviformis*	*Cocconeis distans*	*Navicula* spp.	
Chaetoceros Phaeoceros spp.	*Actinoptychus vulgaris*		*Cocconeis fluminensis*	*Rhopalodia* spp.	
Nitzschia spp.	*Asteromphalus* spp.	*Thalassionema nizschioides* var *nitzschioides*	*Cocconeis scutellum*	*Synedra* spp.	
Nitzschia bicapitata	*Biddulphia* spp.		*Diploneis* spp.		
Nitzschia braarudii	*Coscinodiscus* spp.		*Eunotogramma* spp.		
Nitzschia interruptestriata	*Coscinodiscus centralis*		*Gomphonema* spp.		
Nitzschia sicula	*Coscinodiscus decrescens*		*Opephora marina*		
Planktonellia sol	*Coscinodiscus radiatus*		*Pleurosigma* spp.		
Proboscia spp.	*Cyclotella* spp.		*Surirella* spp.		
Pseudosolenia calcaravis	*Cyclotella caspia*		*Trachyneis aspera*		
Rhizosolenia spp.	*Cyclotella striata*				
Rhizosolenia acuminata	*Cyclotella litoralis/stylorum*				
Rhizosolenia bergonii	*Cymatotheca* spp.				
Rhizosolenia clevei	*Fragilariopsis doliolus*				
Rhizosolenia setigera	*Hemidiscus cuneiformis*				
Roperia tessalata	*Paralia sulcata*				
Thalassionema bacillare	*Pseudo-Nitzschia* spp.				
Thalassionema frauenfeldii	*Trigonium* spp.				
Thalassionema nitzschioides var *parva*					
Thalassiosira spp.					
Thalassiosira eccentrica					
Thalassiosira leptopus					
Thalassiosira oestrupii					
Thalassiothrix spp.					

CPD
7, 2445–2476, 2011

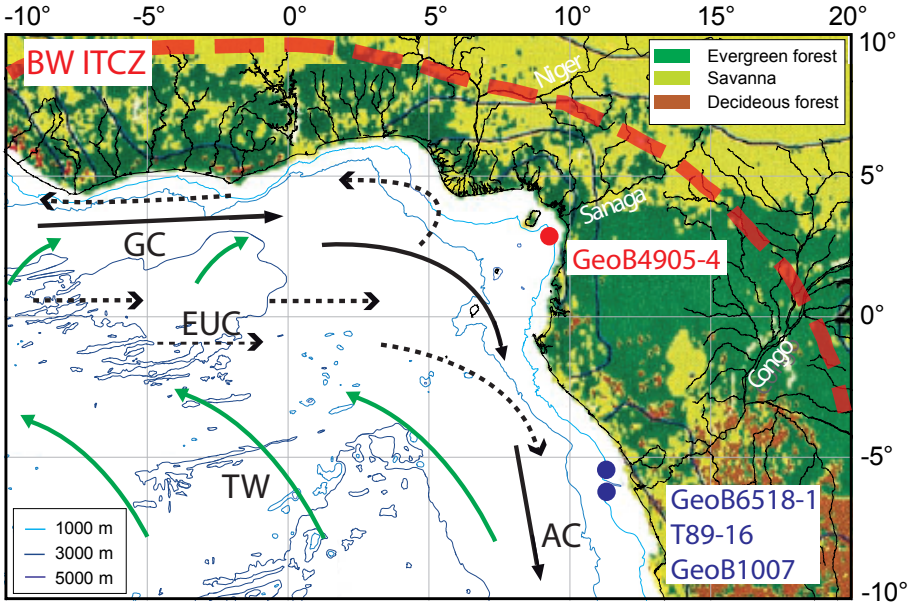

Fig. 1. Bathymetric map of the Gulf of Guinea displaying location of core GeoB4905-4 and other reference sites, along with main surface (plain black arrows) and subsurface currents (dashed black arrows), main atmospheric circulation (green arrows), position of the boreal winter ITCZ (red dashed line), main rivers flowing into the Gulf of Guinea and vegetation distribution in western equatorial Africa (Foley et al., 2003). The boreal winter ITCZ is located around 15–20° N, out of the figure. GC: Guinea Current; AC: Angola Current; EUC: Equatorial Undercurrent; TW: Trade Winds.

CPD
7, 2445–2476, 2011

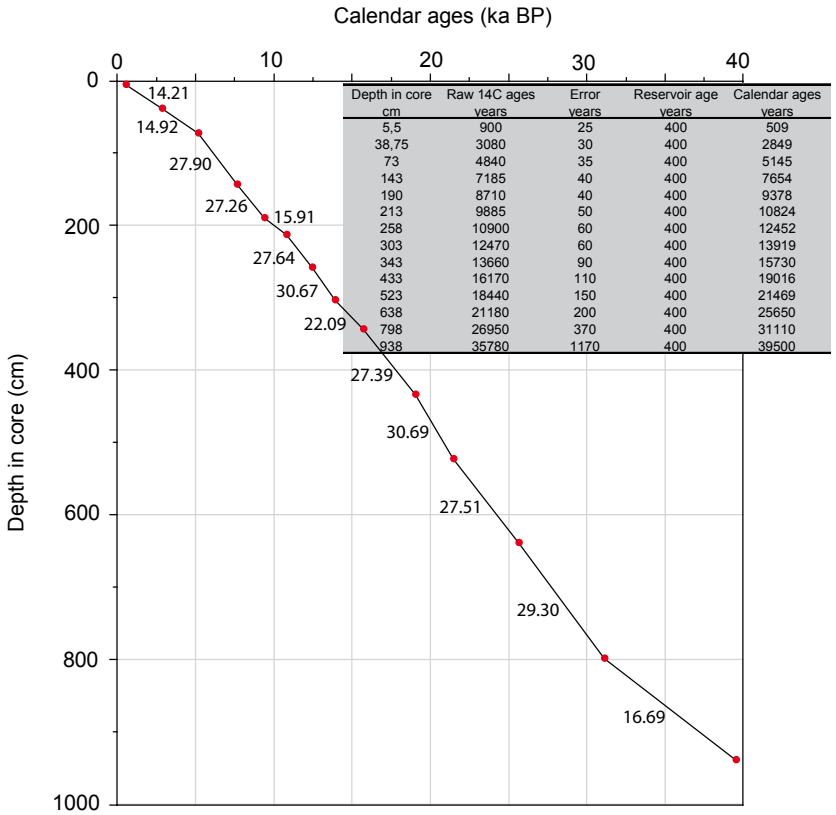

Depth in core cm	Raw 14C ages years	Error years	Reservoir age years	Calendar ages years
5,5	900	25	400	509
38,75	3080	30	400	2849
73	4840	35	400	5145
143	7185	40	400	7654
190	8710	40	400	9378
213	9885	50	400	10824
258	10900	60	400	12452
303	12470	60	400	13919
343	13660	90	400	15730
433	16170	110	400	19016
523	18440	150	400	21469
638	21180	200	400	25650
798	26950	370	400	31110
938	35780	1170	400	39500

Fig. 2. Age model of core GeoB4905-4. The table details the different steps taken to develop an age-model from raw ^{14}C dates to calibrated ages. The graph depicts calibrated ages versus depth. The line depicts the linear interpolation between two consecutive ages. More details can be found in Adegbie et al. (2003) and Weldeab et al. (2005). Numbers associated with the curve represent sedimentation rates in cm ka^{-1}.

CPD
7, 2445–2476, 2011

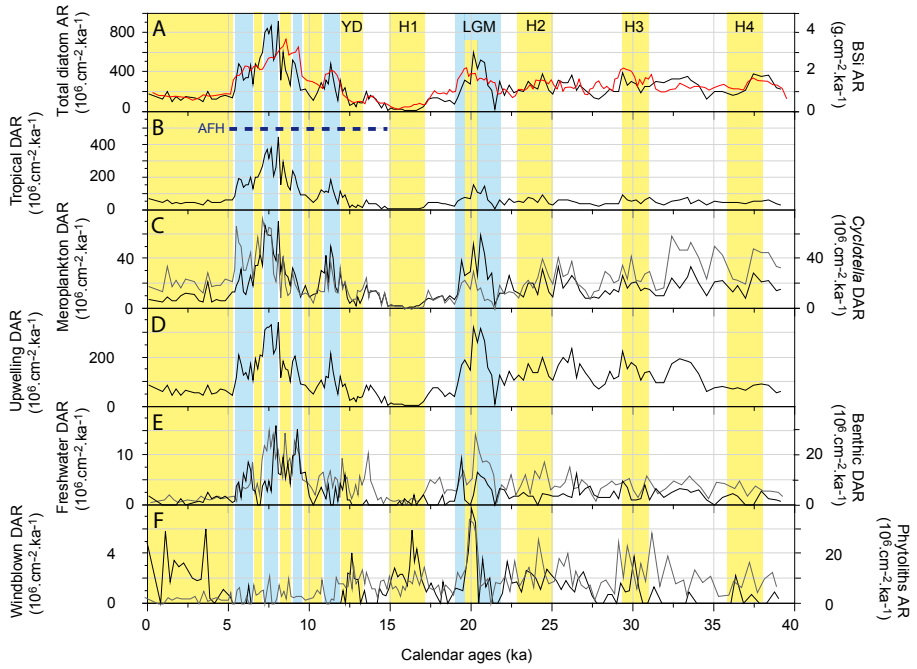

Fig. 3. Accumulation rates of diatoms and biogenic silica in core GeoB4905-4 versus calendar ages. **(A)** – Total diatom accumulation rates (black line) and BSi accumulation rates (red line), **(B)** – accumulation rates of tropical diatoms, **(C)** – accumulation rates of meroplanktonic diatoms (black line) and *Cyclotella* spp. (grey line), **(D)** – accumulation rates of upwelling related diatoms, **(E)** – accumulation rates of freshwater diatoms (black line) and benthic diatoms (grey line) and, **(F)** – accumulation rates of *Aulacoseira* spp. (black line) and opal phytoliths (grey line). Blue and yellow shading represents periods of inferred high precipitations and low precipitations over western Africa, respectively.

CPD
7, 2445–2476, 2011

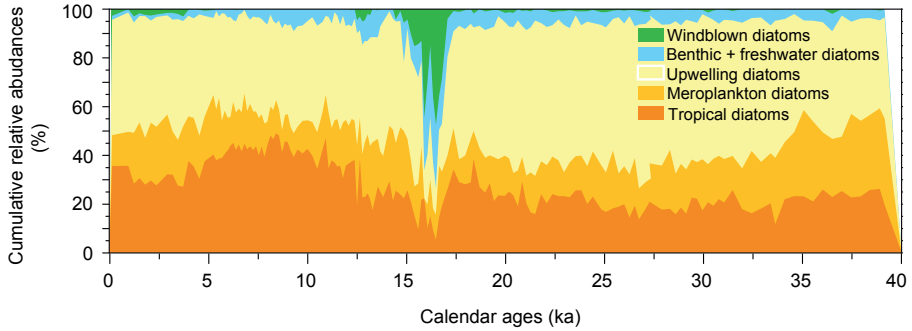

Fig. 4. Cumulative relative abundance of the five diatom groups in core GeoB4905-4 versus calendar ages.

CPD
7, 2445–2476, 2011

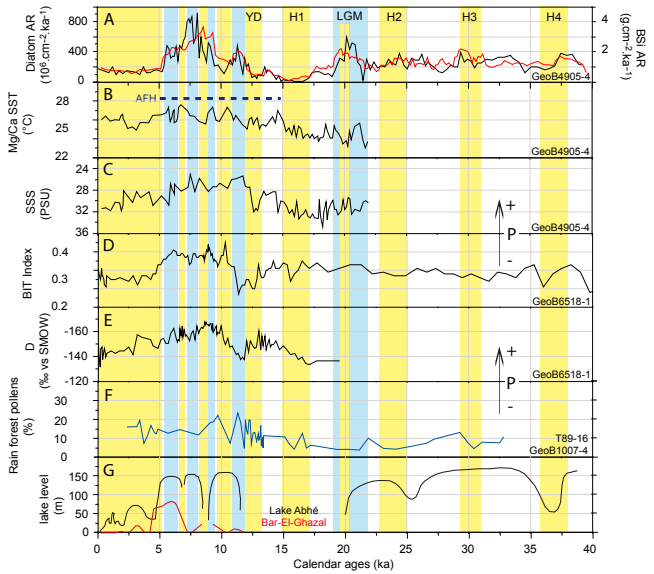

Fig. 5. Comparison of diatom and biogenic silica accumulation rates recorded in core GeoB4905-4 with climate proxies from Equatorial Africa. **(A)** – Total diatom accumulation rates (black curve) and biogenic silica accumulation rates (red curve), **(B)** – eastern Equatorial Atlantic sea-surface temperatures based on Mg/Ca ratios in *Globigerinoides ruber* (Weldeab et al., 2007), **(C)** – eastern Gulf of Guinea salinities calculated using the $\delta^{18}O_{sw}$-SST-SSS relationship suggested for eastern low latitude Atlantic (Weldeab et al., 2005), **(D)** – BIT index tracing the input of continental organic carbon to the eastern equatorial Atlantic (Weijers et al., 2009), **(E)** – relative changes in central African humidity based on δD values of plant wax n-C_{29} alkanes (Schefuss et al., 2005), **(F)** – proportion of lowland rainforest pollens in cores T89-16 and GeoB1007-4 (Marret et al., 2008), **(G)** – lake level height above present level in Lake Abhé (11°05′ N–41°50′ E, black curve) and Bar-El-Ghazal (18° N–17° E, red curve) (Gasse, 2000). Locations of cores are quoted in Fig. 1. *P*: inferred precipitations over western Equatorial Africa.

CPD
7, 2445–2476, 2011